ACS OMEGA

http://pubs.acs.org/journal/acsodf

Article

Molecular Dynamic Simulation of Ni−Al Alloy−H_2O Reactions Using the ReaxFF Reactive Force Field

Jianming Yang,* Yuanbo Zheng, Jian Shi, Yifan Jia, Jialin Li, Qian Zhang, Weiqiang Wang, and Qinwei Yu

Cite This: *ACS Omega* 2023, 8, 9807−9814

Read Online

ACCESS | Metrics & More | Article Recommendations

ABSTRACT: Hydrogen as clean energy can effectively solve the problems of fossil energy shortage and environmental pollution. However, traditional methods of H_2 production are generally lacking in application value. The procedure for manufacturing H_2 by a reaction between active metals and H_2O has received wide attention due to its high efficiency. Profound insights into the mechanism and influencing factors of H_2 production from active metals are insufficient. The ReaxFF reaction force field module of the Amsterdam Modeling Suite (AMS) is applied in this paper to simulate the reaction of Ni−Al alloys with H_2O. It reveals the reaction route of H_2 production at the atomic level. The calculation results show that Al is the most critical active site. Moreover, the H_2 production capacity of the alloy varies with the crystal structure and atomic ratio. The H_2 production rate decreases due to the influence of the water solvation layer and surface coverage. Oxygen reduces the H_2 production capacity because oxygen reduces the active sites for H_2O adsorption by forming a stable oxide layer with Al.

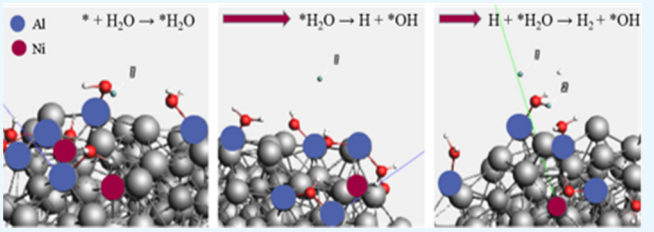

INTRODUCTION

With the world's population growth and rapid economic development, the consumption and demand for energy are gradually increasing. However, the current energy consumed is mainly traditional fossil energy, bringing severe environmental pollution. In recent years, there has been a severe shortage of fossil energy, so it is urgent to find renewable and clean new energy. Hydrogen is the most promising renewable and clean new energy to replace traditional fossil energy because of its high combustion efficiency and benefit to the environment.[1]

Hydrogen is scarce on earth, so it is necessary to produce H_2 from fossil fuels, H_2O, and other hydrogen-containing compounds.[2] At present, there are several methods of H_2 production.[3] (1) Biology produces H_2.[4,5] Cyanobacteria and microalgae can produce H_2 by the action of hydrogenase. However, this method is unstable, and the efficiency is very low. (2) Electrolysis of water produces H_2.[6−8] Although this method is simple, the electricity consumed is far more valuable than the hydrogen produced. (3) Hydrogen is produced from fossil fuels. It is the primary method with mature technology, but there are shortcomings of fuel shortage and emission of a large of CO_2.[9] In recent years, H_2 production by chemical reactions of reactive metals such as magnesium and aluminum has received increasing attention.[10] The response of water or hydrocarbons with reactive metals generates large amounts of hydrogen rapidly, making it possible to produce hydrogen on demand and solve the challenge of hydrogen storage.[11,12]

Al is the most promising for H_2 production among the reported active metals due to its dynamic chemical properties and high energy density.[13−15] However, the strong affinity of Al leads to the rapid formation of an Al_2O_3 film, which limits the reaction with H_2O.[16] Jiang prepared a $La_{1.8}Ti_{0.2}MgNi_{8.7}Al_{0.3}$ alloy with good hydrogen storage and production properties by the melting and annealing method.[17] The Mg−Ni−Y−Al alloy composed by Luo significantly improved H_2 production and electrochemical properties.[18]

Ni−Al alloys have been used for H_2 storage and production,[19−21] but the effect of the reaction mechanism has not been investigated. Therefore, we investigated the mechanism and influencing factors of Ni−Al with H_2O by the Reaxff reaction force field under the Amsterdam Modeling Suite (AMS) chemical simulation platform.[22−24] Al is the adsorption site of O and Ni is the adsorption site of H. The generation of H_2 is mainly through removing H from the $*OH_2$ adsorbed by Al. The addition of Ni will inhibit the generation of H_2 because it tends to form stable adsorption structures such as $AlONiH_2$ and Al_2ONiH. In addition, O_2 will

Received: September 25, 2022
Accepted: December 8, 2022
Published: March 9, 2023

poison the Ni−Al alloy, which dramatically affects the H_2 production capacity of the alloy.

COMPUTATIONAL METHODS

The Reaxff module is a relevant force field on chemical bonding that reasonably describes bond breaking and formation.[25] In addition, it can reasonably model chemical and nonchemical bond interactions such as van der Waals forces and Coulomb interactions.[26−28] This force field provides a system to perform the computational requirements of the simulation and can be used to describe the full range of chemical processes of a reaction.[29] The CHOFeAlNiCuS.ff force field was chosen to investigate the mechanism because it reasonably describes the chemical bond formation and breakage between the atoms of Ni, Al, H, and O.[30] Since the alloy structure cannot be established under the Reaxff module, the Ni−Al alloys used in this paper were obtained from the Inorganic Crystal Structure Database (ICSD). The specific Ni−Al alloy information is shown in Table 1, including the ICSD card number, Ni−Al atomic ratio, and crystal structure.

Table 1. Information on Ni−Al Alloys in the ICSD Crystal Database

number	ICSD number	Ni−Al atomic ratio	crystal structure
Ni−Al-1	58037	1:1	cubic
Ni−Al-2	608784	1:1	tetragonal
Ni−Al-3	107713	2:3	rhombohedral
Ni−Al-4	107937	2:3	trigonal
Ni−Al-5	58038	3:1	cubic
Ni−Al-6	58040	1:3	cubic

The simulations were performed as follows. (1) The Ni−Al alloy clusters were built with a cluster radius of about 0.75 nm and several of about 150 atoms. (2) The clusters are annealed because the established clusters are intercepted from large crystals, and edge effects exist. The annealing process is achieved by setting NVT parameters (constant atomic number and volume with temperature variation), where the cluster temperature is first raised to 900 K (below the melting point of the Ni−Al alloy) and then lowered to 10 K. The cycle is repeated several times, with the atoms rearranging on the cluster surface throughout the process, minimizing the energy. (3) A box with a size of 27 nm^3 is set at the center of the cluster. Then, H_2O molecules are added, which will be randomly distributed inside this box. Next, the cluster and H_2O are divided into two regions, with the cluster set as region one and the added molecules as region 2. To promote the rate of reaction and separation, the NVT temperature is set to 1400 K. However, 1400 K will cause the Ni−Al alloy to move toward the molten state. To maintain the integrity of the Ni−Al alloy clusters, the cluster temperature was set to 10 K. Different temperatures were set in the two regions, 10 K for region 1 and 1400 K for region 2. (4) We used a time step of 0.25 fs, a relatively moderate value that does not need to be changed. The damping constant set for the calculation in this paper is 5 fs and the thermostat is NHC.

Five simulation scenarios were used to investigate the mechanism and influencing factors of the reaction. (1) To investigate the process of H_2O adsorption and H_2 production, an alloy with a Ni−Al atomic ratio of 1:3 and a simple cubic crystal structure was selected. 20 H_2O molecules were added to the established reaction box to investigate the reaction mechanism of H_2 production by the H atom tracking method. (2) Several Ni−Al alloys with crystal structures were retrieved from the ICSD inorganic crystal structure database, and the effect of crystal structure was explored by designing two simulation scenarios. The first scheme selected two alloys with different crystal structures with Ni−Al atomic ratios of 1:1 numbered Ni−Al-1 and Ni−Al-2. The second scheme selected two alloys with different crystal structures with Ni−Al atomic ratios of 2:3, numbered Ni−Al-3 and Ni−Al-4. Other simulation conditions were kept consistent (100 H_2O). (3) Alloys with different Ni−Al atomic ratios of the same crystal structure were chosen to explore the effect of the Ni−Al atomic ratio. The common Ni−Al alloys with atomic ratios of 1:3, 1:1, and 3:1[31] were retrieved from the ICSD with the same crystal structure, numbered Ni−Al-6, Ni−Al-1, and Ni−Al-5. (4) Alloy 58040 was selected, and the effect of adding different H_2O molecules was investigated. (5) Alloy 58040 was selected to investigate the effect of oxygen by adding 100 H_2O and different numbers of O_2.

RESULTS AND DISCUSSION

To determine the appropriate parameters for the simulations, alloy 58040 was modeled by creating a cluster of 150 atoms and adding 100 H_2O inside the box to perform the simulations, as shown in Figure 1a. The results show that the added H_2O is adsorbed on the surface of the cluster at 50,000 steps and 25 ps reaction time and a certain number of H_2 is produced, as shown in Figure 1b.

Compared with the adsorption process of H_2O, the H_2 production process is slower. After 200,000 steps and 100 ps of the reaction, a large amount of H_2 is generated. The H_2O stripped of H is adsorbed on the cluster surface, as shown in Figure 1c. The number of H_2 and energy changes during the whole reaction process are shown in Figure 2. After 200,000 steps and 100 ps of the reaction, the number of generated H_2 reaches a particular value. The energy remains the same

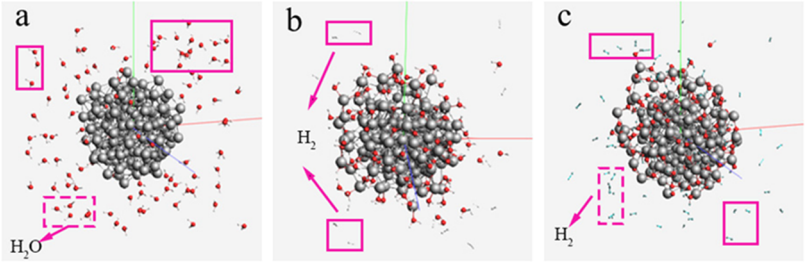

Figure 1. Reaction history of the Ni−Al-6 alloy with H_2O ((a) 0 ps, (b) 50 ps, and (c) 100 ps).

https://doi.org/10.1021/acsomega.2c06188
ACS Omega 2023, 8, 9807−9814

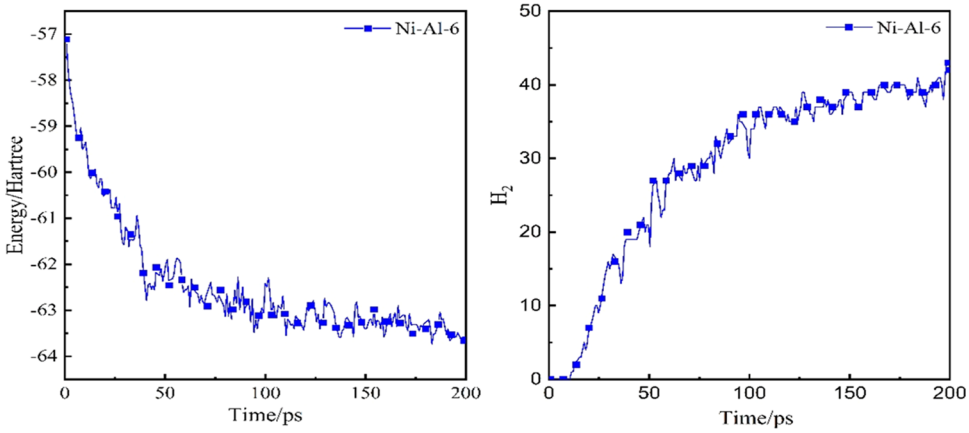

Figure 2. Reaction of Ni−Al-6 with water to produce H_2.

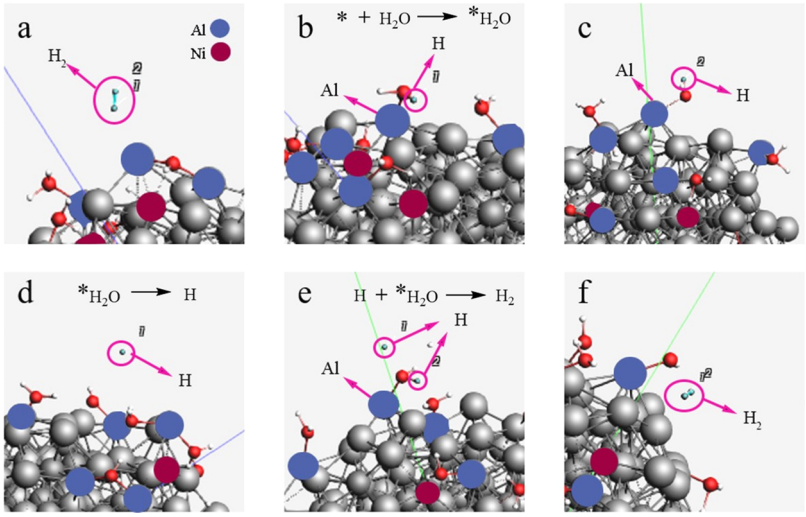

Figure 3. H_2 production process of the Ni−Al alloy reacting with H_2O ((a) H tracking and (b−f) H_2 production process).

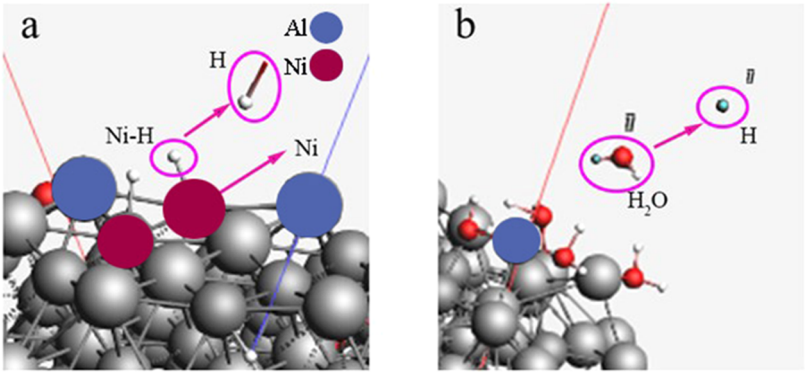

Figure 4. H_2 production process of the Ni−Al alloy reacting with H_2O ((a) Ni−H and (b) H_2O dehydrogenation).

because the Ni−Al alloy forms a more stable adsorption structure after reacting with H_2O.

Based on the above calculations, the reaction step was determined to be 400,000 and the time was 200 ps. In this range, it can ensure the complete reaction of the alloy with H_2O, and the amount of H_2 generation remains the same.

Basic Principle of the Ni−Al Reaction with H_2O. The Ni−Al-6 alloy was used to investigate the mechanism of H_2 production. The reaction mechanism was determined by adding 20 H_2O to a 150 atoms cluster box and observing the mechanism using the H tracking method, which can be divided into three different H_2 production mechanisms based on the different ways of H production. Al on the cluster surface in the Ni−Al alloy is an adsorption site for the O atom, and Ni has a good adsorption effect on H. The mechanism of the first kind of H_2 production is shown in Figure 3. First, H_2O is adsorbed by Al to form an $*OH_2$ structure. The adsorbed $*OH_2$ structure will take off H to create a free-state H due to the relatively stable Al−O bond, as shown in Figure 3d. The free-

https://doi.org/10.1021/acsomega.2c06188
ACS Omega 2023, 8, 9807−9814

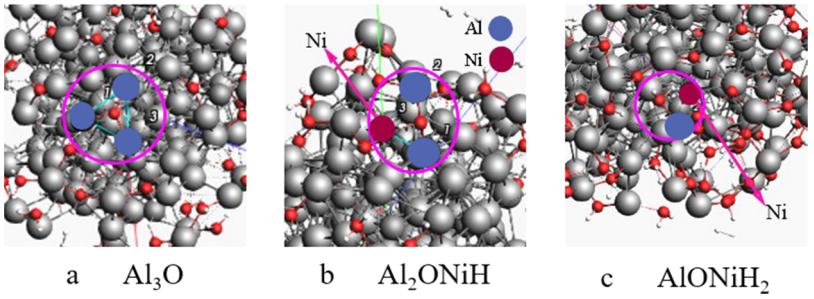

Figure 5. Stable structure formed by the reaction of the Ni−Al alloy with H_2O ((a) Al_3O, (b) Al_2ONiH, and (c) $AlONiH_2$).

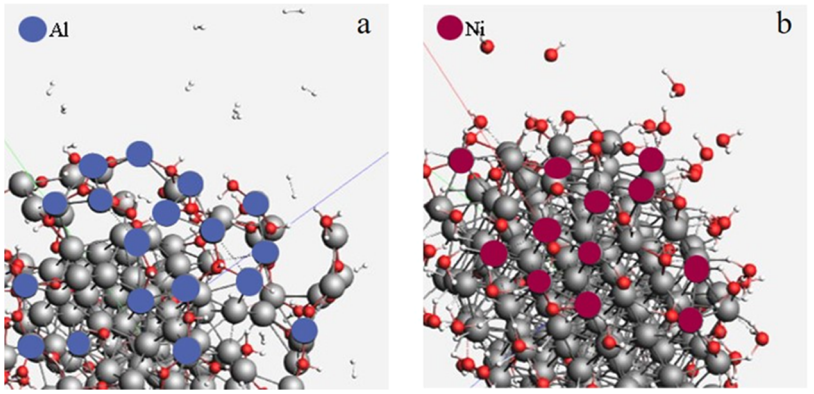

Figure 6. Reaction history of Al and Ni with H_2O ((a) pure Al and (b) pure Ni).

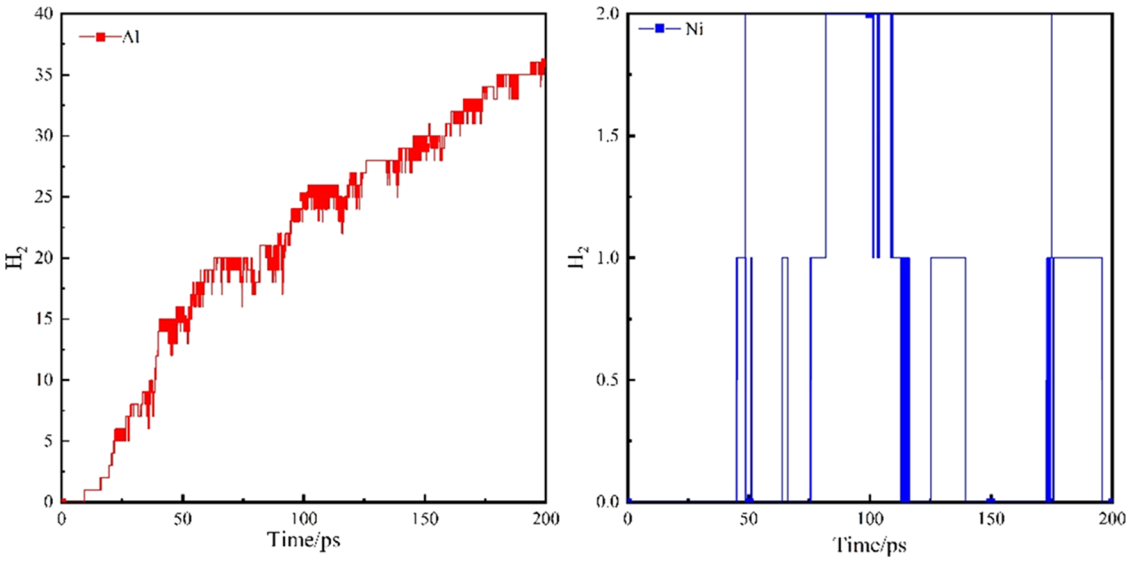

Figure 7. Reaction of Al and Ni with H_2O to produce H_2.

state H will interact with $*OH_2$ to make $*OH_2$ dehydrogenation to generate H_2.

The primary reaction mechanism of H_2 is $*OH_2$ dehydrogenation. Figure 4 shows other processes which produce a small number of H atoms. Figure 4a shows that the adsorbed-state $*OH_2$ structure formed first and adjacent Ni atoms adsorb the H on $*OH_2$. Then, the O−H bond is broken to begin *H adsorption by Ni atoms alone. Finally, *H dehydrogenates into free-state H for H_2 generation. Figure 4b shows that the free-state H_2O molecules are directly dehydrogenated to produce H atoms.

During the reaction of the Ni−Al alloy with H_2O, the adsorbed H_2O will shed different amounts of H to form other stable structures due to the different positions of the cluster surface, as shown in Figure 5. Figure 5a shows H_2O shedding two H atoms, and Al adsorbs the remaining O atom to form Al_3O or the Al−O−Al structure. Figure 5b shows H_2O shedding one H atom to create Al_2ONiH, Al_3ONiH, AlONiH, etc. Figure 5c shows the $AlONiH_2$ structure formed by H_2O without shedding H atoms. In conclusion, the reaction process will generate H_2 by the process of $*OH_2$ or *H dehydrogenation. Due to the higher activity of Al than Ni, the reaction process is dominated by the $*OH_2$ dehydrogenation adsorbed

https://doi.org/10.1021/acsomega.2c06188
ACS Omega 2023, 8, 9807−9814

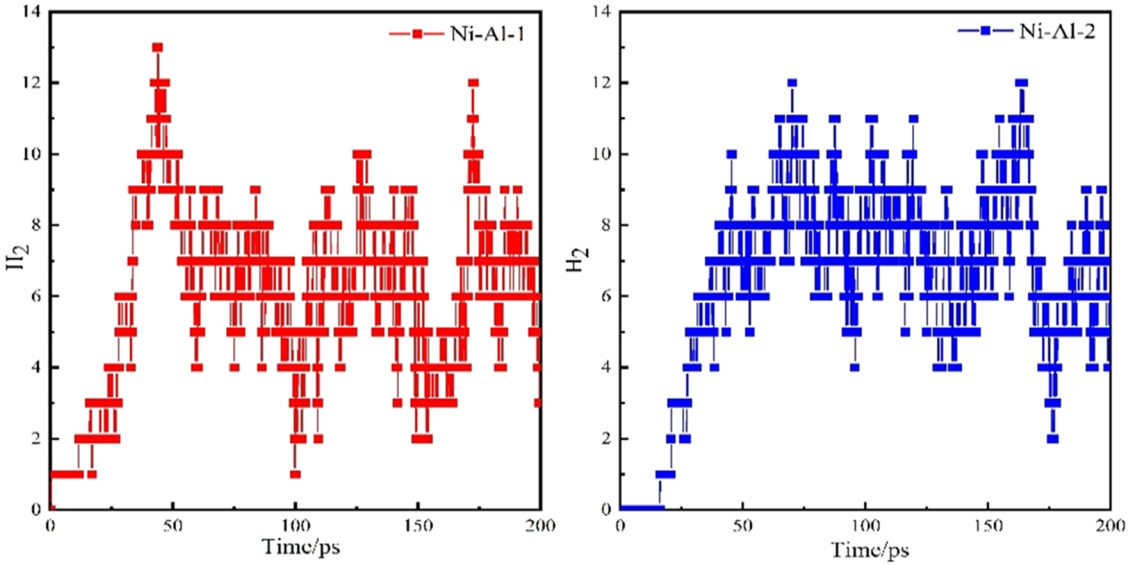

Figure 8. H_2 production diagram of different crystal structures with an atomic ratio of 1:1.

by Al. Eventually, all of them will form a particular form of a stable structure, where the generation of H_2 reaches a maximum, and the energy of the system reaches a minimum.

The results were verified for Al and Ni alone under the same force field and simulation conditions, and the results are shown in Figures 6 and 7. As can be seen from Figure 6a,b, Al is the active adsorption site for O and Ni is the active adsorption site for H, which is consistent with the conclusions obtained from the simulation calculations for the Ni−Al alloy. The number of H_2 generations is shown in Figure 7. Al alone produces a large amount of H_2 and Ni produces almost no H_2 which indicates that H_2 is mainly generated through H_2O adsorbed by Al, $*OH_2$ dehydrogenation, which is also consistent with the results of Ni−Al alloy simulation calculations. Through the simulation calculation of Al, Ni with H_2O, not only the accuracy of the results of the Ni−Al alloy is confirmed but also the applicability of the used force field is verified.

Effect of the Crystal Structure of Different Ni−Al Alloys. Simulations were carried out for alloys with different crystal structures of Ni−Al atomic ratios of 1:1 and 2:3. Figure 8 shows the results of H_2 production for two other crystal structures with atomic ratios of 1:1. The Ni−Al-1 crystal structure is simple cubic and the Ni−Al-2 crystal structure is a simple square. The results show that the rate of H_2 production and the number of H_2 generated are basically the same, and the number of H_2 generated is around 8. The simulated data of another set of atomic ratios of 2:3, the Ni−Al-3 crystal with a rhombohedral lattice and the Ni−Al-4 crystal with a triangular lattice. The results show that the H_2 production rate is the same and the H_2 generation number of Ni−Al-3 is higher than that of Ni−Al-4. As shown in Figure 9, the number of H_2 generated by Ni−Al-3 is around 20, while Ni−Al-4 only generates about 10.

The reason is explored by the surface atoms of different alloy clusters. Figure 10 shows the surface atoms distribution of Ni−Al-1 and Ni−Al-2 clusters. Ni and Al are the same for both structures. In contrast, the surface atomic numbers of Ni−Al-3 and Ni−Al-4 are pretty different. Although there are only 80 atoms on the surface of Ni−Al-3, the number of Al reaches 57, and the number of Ni atoms is 23, adsorbing 160 H. However, the number of Al atoms on the surface of Ni−Al-4 is the same,

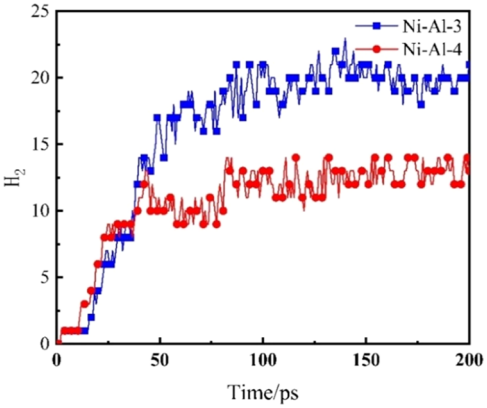

Figure 9. H_2 production diagram of different crystal structures with an atomic ratio of 2:3.

and the number of Ni reaches 39, adsorbing 180 H. By comparison, the H_2 production numbers of Ni−Al-1 and Ni−Al-2 are the same, which is attributed to the consistent number of Al and Ni atoms on the surface. The H_2 produced by Ni−Al-4 is significantly lower than Ni−Al-3 because the number of Ni atoms on its surface is higher than Ni−Al-3. Ni is a highly active adsorption site for H, which leads to the reduction of the number of H_2O dehydrogenated and tends to form stable structures such as $AlONiH_2$ and Al_2ONiH. There is no difference in H_2 production rates due to the fact that the number of surface active Al atoms is high enough to preferentially carry out the process of $*OH_2$ dehydrogenation to generate H_2.

The results show no difference in the H_2 production capacity of simple cubic and orthorhombic Ni−Al alloys. However, the H_2 production capacity of a simple trigonal crystal structure is significantly higher than that of a triangular lattice because different crystal structures affect the number of atoms of Ni−Al and the chemical environment (edges, angles, vertices, etc.). In conclusion, alloy clusters with different crystal structures have distinct surface atomic numbers and chemical environments, resulting in various H_2 production capacities for reactions with H_2O.

https://doi.org/10.1021/acsomega.2c06188
ACS Omega 2023, 8, 9807−9814

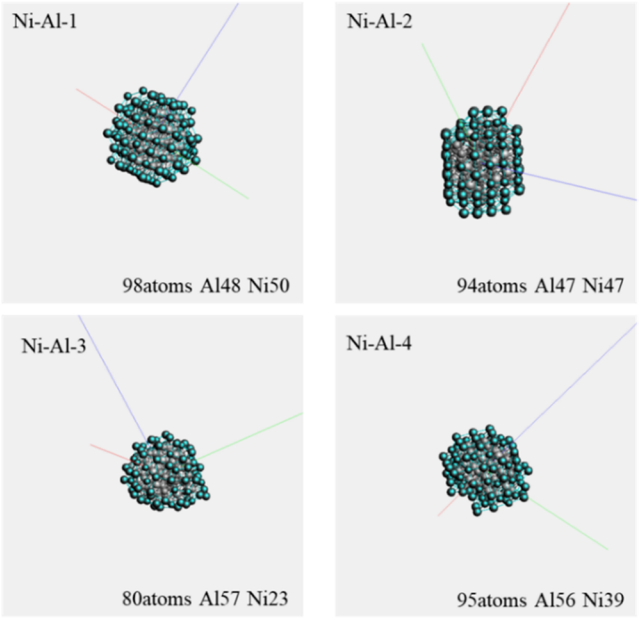

Figure 10. Atom distribution on the surface of alloy clusters with different crystal structures.

Effect of Different Ni−Al Atomic Ratios. The same crystal structure alloys with different Ni−Al atomic ratios were selected for the simulations, and the Ni−Al atomic ratios were 1:3, 1:1, and 3:1, respectively. The results are shown in Figure 11. When the Ni−Al atomic ratios are 3:1 and 1:1, the H_2 production activity is low. While the ratio is 1:3, the H_2 production activity increases substantially. Therefore, the H_2 production capacity and the H_2 production rate increase significantly as the Ni−Al atomic ratio decreases.

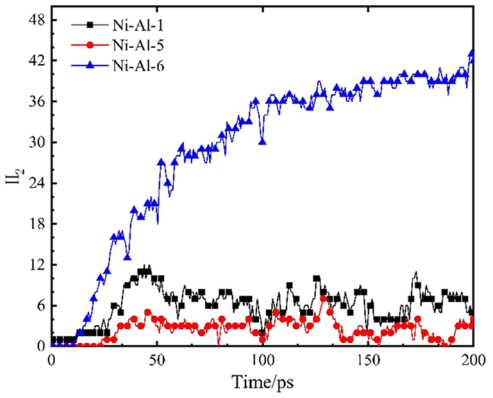

Figure 11. H_2 production with different Ni−Al atomic ratios.

Figure 12 shows the number of Ni and Al atoms on the surface of the three scaled alloys. The number of Al atoms on the surface of the Ni−Al-6 cluster is significantly higher than Ni−Al-1 and Ni−Al-5, which indicates that the $*OH_2$ dehydrogenation process dominates the H_2 production process by Al adsorption. The difference in the number of H_2 production between Ni−Al-1 and Ni−Al-5 is insignificant because Ni−Al 5 has more Ni atoms on the surface. Some H_2 generation reaction occurs through *H desorption by Ni adsorption, but the number of H_2 generation by this process is lower than $*OH_2$ generation by Al adsorption.

By comparison, the H_2 production activity of Al is higher than Ni. The higher the number of Al atoms on the surface, the more favorable it is for H_2 production. The excessive number of Ni atoms will produce H_2 through the desorption of *H, but it is easier to form stable adsorption structures such as $AlONiH_2$ and Al_2ONiH, which inhibit the desorption process of $* OH_2$. In summary, the rate and the number of H_2 production increase substantially when the Ni−Al atomic ratio is lower. The H_2 production capacity decreases considerably as the ratio increases, which is attributed to the decrease of the $*OH_2$ desorption process and the inhibition of the H_2 production reaction by Ni.

Simulation of Different Numbers of H_2O. The Ni−Al-6 alloy with a high H_2 production activity was selected, and the results were calculated by adding different numbers of H_2O, as shown in Figure 13. With the increase of H_2O, the H_2 production rate gradually increased and the number of H_2 produced also steadily increased. However, the H_2 production proportion was the first to rise and then decrease, as shown in Figure 13b. The H_2 production proportion reaches a maximum when the number of H_2O is about 50. In contrast, the H_2 production proportion decreases significantly when H_2O increases or decreases.

The results of the H_2 production rate and the number generated show that the increase of H_2O benefits the reaction. When the number of H_2O is lower, it is more challenging to dehydrogenate H_2O adsorbed by the active sites, which tend to form stable structures such as $AlONiH_2$ and Al_2ONiH_2. With the increase of H_2O, there are more active sites to adsorb H_2O. The adjacent active sites are basically in this state, and it isn't easy to adsorb the same H_2O together with the adjacent active sites. Therefore, $*OH_2$ is easier to dehydrogenate, and the rate of H_2 production and the number of H_2 generated gradually increase. The bottom H_2 production proportion under a small number of H_2O is due to the high availability of surface atoms causing too many adsorbed H_2O, resulting in an insufficient H_2O solventized layer to assist $*OH_2$ dehydrogenation, forming stable structures such as $AlONiH_2$, Al_2ONiH_2. When the number of H_2O is too high, most H_2O is adsorbed to the clusters, and the surface coverage reaches saturation,

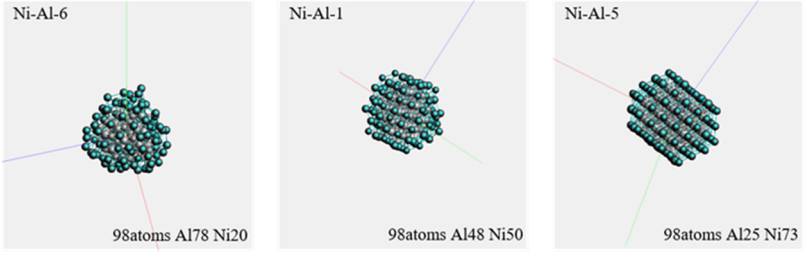

Figure 12. Atom distribution on the surface of alloy clusters with different Ni−Al atomic ratios.

https://doi.org/10.1021/acsomega.2c06188
ACS Omega 2023, 8, 9807−9814

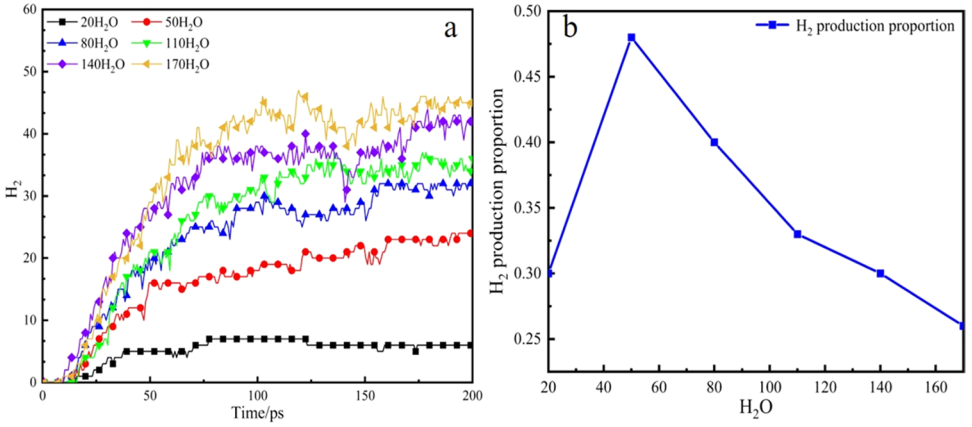

Figure 13. Simulation results of different H_2O ((a) number of H_2 produced and (b) H_2 production proportion).

hindering $*OH_2$ dehydrogenation, which is the self-poisoning phenomenon of Ni−Al alloys.[32]

Effect of O_2. As mentioned above, one of the main obstacles to H_2 generation is the difficulty for the clusters to recover their original state after the reaction and exist in a stable adsorbed-state structure, which is due to the high activity of Al that quickly forms a strong chemical bond with O, forming an oxide layer that reduces the available sites for H_2O adsorption and decomposition. Figure 14 shows the

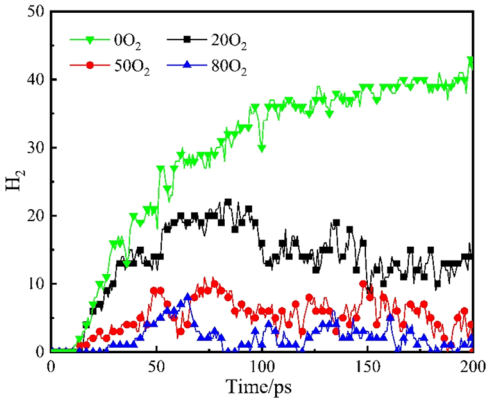

Figure 14. Simulation results of different O_2.

results of simulation calculations with the addition of different molecular numbers of O_2. The rate of H_2 production and the number of H_2 decrease substantially with the increase of O_2.

Because of the highly active adsorption of Al on O in Ni−Al alloys, the addition of O_2 will occupy most of the active sites and form a stable oxide layer, which reduces the adsorption of H_2O. This effect will be more evident with the increase in O_2. It can also be shown that the Ni−Al alloy has a higher adsorption effect on O_2 than H_2O. In the presence of O_2, it will preferentially react with O_2 to form a stable oxide layer, which is the toxic effect of oxygen on Ni−Al alloys.

CONCLUSIONS

It is shown that the reaction of Ni−Al alloys with H_2O is mainly the dehydrogenation of the $*OH_2$ structure formed by Al adsorption, and a small part of H_2 is generated by the dehydrogenation of *H adsorbed by Ni. At the end of the reaction, Al-adsorbed O and Ni-adsorbed H form a stable structure. The active sites are occupied, and the number of H_2 generations remains stable. Alloy clusters with different crystal structures and Ni−Al atomic ratios have different numbers of Al atoms on the surface, resulting in a highly diverse activity. By adding different initial amounts of H_2O, it was concluded that an optimal dose exists based on alloy clusters. When there is too little H_2O, all cluster surface atoms will adsorb H_2O and tend to form $*OH_2$ stable structures. When there is too much H_2O, H_2O will lead to surface saturation and hinder the dehydrogenation of $*OH_2$ facilities. In addition, the formation of oxide layers leads to the loss of available surface reaction active sites, resulting in a decrease in the H_2 production rate.

Reactive metal Al with H_2O produces large amounts of H_2, but an oxide layer forms in the air, covering the active sites and inhibiting H_2 production. Therefore, understanding how to prevent the formation of this oxide layer is essential for developing this H_2 production technology. Adding the right amount of Ni atoms inhibits the rate of H_2 production and makes on-demand H_2 production. In the future, further research using various metal alloys is needed to develop a method to prevent the formation of this firmly bound oxide layer and to achieve precise regulation of the rate and amount of H_2 production.

AUTHOR INFORMATION

Corresponding Author

Jianming Yang − *State Key Laboratory of Fluorine & Nitrogen Chemicals, Xi'an Modern Chemistry Research Institute, Xi'an 710065, P. R. China;* orcid.org/0000-0001-5177-9649; Email: yangjm204@163.com

Authors

Yuanbo Zheng − *State Key Laboratory of Fluorine & Nitrogen Chemicals, Xi'an Modern Chemistry Research Institute, Xi'an 710065, P. R. China*

Jian Shi − *State Key Laboratory of Fluorine & Nitrogen Chemicals, Xi'an Modern Chemistry Research Institute, Xi'an 710065, P. R. China;* orcid.org/0000-0002-2896-3613

Yifan Jia − *State Key Laboratory of Fluorine & Nitrogen Chemicals, Xi'an Modern Chemistry Research Institute, Xi'an 710065, P. R. China*

Jialin Li − *State Key Laboratory of Fluorine & Nitrogen Chemicals, Xi'an Modern Chemistry Research Institute, Xi'an 710065, P. R. China*

https://doi.org/10.1021/acsomega.2c06188
ACS Omega 2023, 8, 9807−9814

Qian Zhang − *State Key Laboratory of Fluorine & Nitrogen Chemicals, Xi'an Modern Chemistry Research Institute, Xi'an 710065, P. R. China*

Weiqiang Wang − *State Key Laboratory of Fluorine & Nitrogen Chemicals, Xi'an Modern Chemistry Research Institute, Xi'an 710065, P. R. China*

Qinwei Yu − *State Key Laboratory of Fluorine & Nitrogen Chemicals, Xi'an Modern Chemistry Research Institute, Xi'an 710065, P. R. China*

Complete contact information is available at: https://pubs.acs.org/10.1021/acsomega.2c06188

Notes

The authors declare no competing financial interest.

■ ACKNOWLEDGMENTS

The authors acknowledge financial support from the National Natural Science Foundation of China (Grant Nos: 21902124, 22072112) and the Key Research and Development Projects of Shanxi Province (Grant Nos: 2021GY-115, 2019TD-009).

■ REFERENCES

(1) Dawood, F.; Anda, M.; Shafullah, G. Hydrogen production for energy: An overview. *Int. J. Hydrogen Energy* **2020**, *45*, 3847−3869.

(2) Kannah, Y.; Kavitha, S.; Karthikeyan, P.; Kumar, G.; Dai-Viet, N.; et al. Techno-economic assessment of various hydrogen production methods-A review. *Bioresour. Technol.* **2021**, *319*, No. 124175.

(3) Niaz, S.; Manzoor, T.; Pandith, A. H. Hydrogen storage: Materials, methods and perspectives. *Renewable Sustainable Energy Rev.* **2015**, *50*, 457−469.

(4) Zhang, Y. T.; Fan, X. L.; Yang, Z. M.; Wang, H. Y.; Yang, D. W.; Guo, R. B. Characterization of H_2 photoproduction by a new marine green alga, Platymonas helgolandica var. tsingtaoensis. *Appl. Energy* **2012**, *92*, 38−43.

(5) Dahiya, S.; Chatterje, S.; Sarkar, O.; Mohan, V. Renewable hydrogen production by dark-fermentation: Current status, challenges and perspectives. *Bioresour. Technol.* **2021**, *321*, No. 124354.

(6) Anantharaj, S.; Aravindan, V. Developments and Perspectives in 3d Transition-Metal-Based Electrocatalysts for Neutral and Near-Neutral Water Electrolysis. *Adv. Energy Mater.* **2019**, *10*, No. 1902666.

(7) Grigoriev, S. A.; Fateev, V. N.; Bessarabov, D. G.; Millet, P. Current status, research trends, and challenges in water electrolysis science and technology. *Int. J. Hydrogen Energy* **2020**, *45*, 26036−26058.

(8) Milier, H. A.; Bouzek, K.; Hnat, J.; Loos, S.; Bernäckeret, C. I.; Weißgärber, T.; Röntzsch, L.; Meier-Haack, J. Green hydrogen from anion exchange membrane water electrolysis: a review of recent developments in critical materials and operating conditions. *Sustainable Energy Fuels* **2020**, *4*, 2114−2133.

(9) Zhou, L. Progress and problems in hydrogen storage methods. *Renewable Sustainable Energy Rev.* **2005**, *9*, 395−408.

(10) Eftekhari, A.; Fang, B. Z. Electrochemical hydrogen storage: Opportunities for fuel storage, batteries, fuel cells, and supercapacitors. *Int. J. Hydrogen Energy* **2017**, *42*, 25143−25165.

(11) Pang, Y. P.; Li, Q. A review on kinetic models and corresponding analysis methods for hydrogen storage materials. *Int. J. Hydrogen Energy* **2016**, *41*, 18072−18087.

(12) Hirscher, M.; Yartys, V.; Baricco, M.; Colbe, J. B.; Blanchard, D.; Bowman, R.; Broom, D.; Buckley, C.; Chang, F.; Chen, P.; et al. Materials for hydrogen-based energy storage − past, recent progress and future outlook. *J. Alloys Compd.* **2020**, *827*, No. 153548.

(13) Grosjean, M. H.; Zidoune, M.; Roué, L.; Huot, J. Y. Hydrogen production via hydrolysis reaction from ball-milled Mg-based materials. *Int. J. Hydrogen Energy* **2006**, *31*, 109−119.

(14) Grosjean, M.-H.; Roue, L. Hydrolysis of Mg-salt and MgH_2-salt mixtures prepared by ball milling for hydrogen production. *J. Alloys Compd.* **2006**, *416*, 296−302.

(15) Kravchenko, O. V.; Semenenko, K. N.; Bulychev, B. M.; Kalmykov, K. B. Activation of aluminum metal and its reaction with water. *J. Alloys Compd.* **2005**, *397*, 58−62.

(16) Martínez, S. S.; Benites, W.; Gallegos, A.; Sebastián, P. J. Recycling of aluminum to produce green energy. *Sol. Energy Mater. Sol. Cells* **2005**, *88*, 237−243.

(17) Jiang, W. Q.; Qin, C. S.; Zhu, R. R.; Guo, J. Annealing effect on hydrogen storage property of Co-free $La_{1.8}Ti_{0.2}MgNi_{8.7}Al_{0.3}$ alloy. *J. Alloys Compd.* **2013**, *565*, 37−43.

(18) Cui, N.; Luo, J. T.; Chuang, K. T. Nickel-metal hydride (Ni-MH) battery using Mg Ni-type hydrogen storage alloy. *J. Alloys Compd.* **2000**, *302*, 218−226.

(19) Gu, J.; Zhang, X. P.; Fu, L.; Pang, A. M. Study on the hydrogen storage properties of the dual active metals Ni and Al doped graphene composites. *Int. J. Hydrogen Energy* **2019**, *44*, 6036−6044.

(20) Wang, H. Z.; Leung, D. Y.; Leung, M. K.; Ni, M. A review on hydrogen production using aluminum and aluminum alloys. *Renewable Sustainable Energy Rev.* **2009**, *13*, 845−853.

(21) Takehira, K. "Intelligent" reforming catalysts: Trace noble metal-doped Ni/Mg(Al)O derived from hydrotalcites. *J. Nat. Gas Chem.* **2009**, *18*, 237−259.

(22) Li, G. X.; Lu, Y. J.; Qi, S. T. Investigation of hydrogen oxidation in supercritical H_2O/CO_2 mixtures using ReaxFF molecular dynamics simulation. *J. Supercrit. Fluids* **2020**, *155*, No. 104661.

(23) Huygh, S.; Bogaerts, A.; Duin, A.; Neyts, E. Development of a ReaxFF reactive force field for intrinsic point defects in titanium dioxide. *Comput. Mater. Sci.* **2014**, *95*, 579−591.

(24) He, Z. H.; Li, X. B.; Liu, L. M.; Zhu, W. J. The intrinsic mechanism of methane oxidation under explosion condition: A combined ReaxFF and DFT study. *Fuel* **2014**, *124*, 85−90.

(25) Rahnamoun, A.; Duin, A. C. Reactive molecular dynamics simulation on the disintegration of Kapton, POSS polyimide, amorphous silica, and teflon during atomic oxygen impact using the ReaxFF reactive force-field method. *J. Phys. Chem. A* **2014**, *118*, 2780−2787.

(26) Feng, M. Y.; Jiang, X. Z.; Mao, Q.; Luo, K.; Hellier, P. Initiation mechanisms of enhanced pyrolysis and oxidation of JP-10 (exo-tetrahydrodicyclopentadiene) on functionalized graphene sheets: Insights from ReaxFF molecular dynamics simulations. *Fuel* **2019**, *254*, No. 115643.

(27) Cao, Y.; Liu, C.; Xu, X. X.; Huo, E.; Pu, Y. Influence of water on HFO-1234yf oxidation pyrolysis via ReaxFF molecular dynamics simulation. *Mol. Phys.* **2019**, *117*, 1768−1780.

(28) Chenoweth, K.; Duin, A.; Dasgupta, S.; Goddark, W. Initiation Mechanisms and Kinetics of Pyrolysis and Combustion of JP-10 Hydrocarbon Jet Fuel. *J. Phys. Chem. A* **2009**, *113*, 1740−1746.

(29) Kim, S.; Duin, A.; Kubicki, J. Molecular dynamics simulations of the interactions between TiO_2 nanoparticles and water with Na^+ and Cl^-, methanol, and formic acid using a reactive force field. *J. Mater. Res.* **2012**, *28*, 513−520.

(30) Rahaman, O.; Duin, A.; Goddard, W.; Doren, D. Development of a ReaxFF reactive force field for glycine and application to solvent effect and tautomerization. *J. Phys. Chem. B* **2011**, *115*, 249−261.

(31) Morsi, K. Review: reaction synthesis processing of Ni-Al intermetallic materials. *Mater. Sci. Eng.: A* **2001**, *299*, 1−15.

(32) Russo, M.; Li, R.; Mench, M.; Duin, A. Molecular dynamic simulation of aluminum−water reactions using the ReaxFF reactive force field. *Int. J. Hydrogen Energy* **2011**, *36*, 5828−5835.